INTERNATIONAL JOURNAL OF PRECISION ENGINEERING AND MANUFACTURING Vol. 15, No. 11, pp. 2351-2356 NOVEMBER 2014 / 2351
DOI: 10.1007/s12541-014-0600-x

Multi Objective Optimization of Friction Stir Welding Parameters Using FEM and Neural Network

Mohammad Hasan Shojaeefard[1], Mostafa Akbari[1,#], and Parviz Asadi[2]

1 Department of Automotive Engineering, Iran University of Science and Technology, Tehran, Iran
2 Department of Mechanical Engineering, University of Tehran, Tehran, Iran
Corresponding Author / E-mail: mr.mostafaakbari@yahoo.com, TEL: +9122964858, FAX: +98(21)89773069

KEYWORDS: Friction stir welding, Neural network, Optimization, Finite element method

In this study the inuence of rotational and traverse speed on the friction stir welding of AA5083 aluminum alloy has been investigated. For this purpose a thermo-mechanically coupled, 3D FEM analysis was used to study the effect of rotational and traverse speed on welding force, peak temperature and HAZ width. Then, an Articial Neural Network (ANN) model was employed to understand the correlation between the welding parameters (rotational and traverse speed) and peak temperature, HAZ width and welding force values in the weld zone. Performance of the ANN model was found excellent and the model can be used to predict peak temperature, HAZ width and welding force. Furthermore, in order to find optimum values of traverse and rotational speed, the multi-objective optimization was used to obtain the Pareto front. Finally, the Technique for Order Preference by Similarity to the Ideal Solution (TOPSIS) was employed to obtain the best compromised solution.

Manuscript received: October 25, 2013 / Revised: May 26, 2014 / Accepted: July 16, 2014

1. Introduction

Friction Stir Welding (FSW) has been used to join aluminum alloys,[1,2] Mg,[3] Cu[4] and some of which have been classified as practically unweldable by traditional welding methods. This technique utilizes a non-consumable rotating welding tool to generate frictional heat and cause deformation at the welding zone, thereby affecting the formation of a joint, while the material is in the solid state.[5]

Tool rotational and traverse speeds are very important parameters in friction stir welding. The tool rotation results in stirring and mixing of material and the tool translation flows the stirred material from the leading face of the pin to its trailing face and nishes welding process. The inuence of rotational speed, and traverse speed on the weld properties has been evaluated earlier, but effect of these parameters on HAZ width, welding force and peak temperature has not thoroughly investigated. Akbari and Abdi[2] investigated the influence of rotational and traverse speeds on the friction stir lap joining of 5083 aluminum alloy to brass. Their results indicated that using a high rotational speed or a low traverse speed increased the size of the intermetallic compound area. They stated that increasing the rotational speed firstly increased the tensile shear force to a maximum value, and then a decrease occurred. Shojaeefard et al.[6] performed a sensitivity analysis to investigate effect of the rotational and traverse speed on the tensile shear force in terms of magnitude and direction.

In this investigation in order to investigate the effect of tool rotational and traverse speeds on HAZ width, welding force and peak temperature, a thermo-mechanically coupled, rigid-viscoplastic, fully 3D FEM analysis was used. A number of works made attempts to develop numerical codes for FSW. Buffa et al[7] established a 3D nite element method to simulate friction stir welding using DEFORM-3D. Their model correctly predicts the non-symmetric nature of FSW process, and the relationships between the tool forces and process parameters. Shojaeefard et al.[8] investigated the effect of tool pin and shoulder diameter on welding force, material flow, thermal and strain distributions of friction stir welding using finite element method. Kim et al.[9] performed thermo-mechanical simulation of the friction stir welding using a nite volume method. They assumed the material to be in perfect contact with the tool and rotate at the same speed as the tool. With this full sticking condition at the interface between the tool and the material, heat was generated only by plastic deformation without frictional heat.

Articial neural networks (ANN) are employed to solve different problems in engineering, especially for some areas where the conventional methods fail. Shojaeefard et al.[5] developed an articial

Table 1 Chemical composition of experimental plates (wt%)

Si	Fe	Cu	Mn	Mg	Zn	Ti
0.1	0.31	0.04	0.61	4.27	0.02	0.026

neural network model to predict the mechanical properties of friction stir welding as function of rotational and traverse speed. They claimed that the performance of the ANN model was excellent. Buffa et al.[10] trained an artificial neural network to predict the microhardness values of the welded butt joints for the FSW of Ti-6Al-4V titanium alloy.

In this study the effect of rotational and traverse speed on peak temperature, HAZ width and welding force in friction stir welding of AA5083 aluminum alloy was investigated. In order to investigate the effect of rotational and traverse speed, thermo-mechanically coupled rigid-viscoplastic 3D FEM was employed. Then, an integrated approach using an articial neural network and hybrid-multi-objective optimization is proposed to find optimum values of traverse and rotational speed. Here, ANN was employed to model the relationships between the traverse and rotational speeds and peak temperature, HAZ width and welding force, while the multi-objective optimization was employed to compute Pareto-optimal non-dominated solutions.

2. Experimental Setup

In this study the AA5083 in the form of 6mm-thick sheet was used. The base metal was in annealed condition. The chemical composition of base metal is given in Table 1.

The FSW tool is consists of a cylindrical inserted pin with 3 mm of diameter, 2 mm height, and an 11.5 mm shoulder diameter and rotated with a constant tilt angle of 3°, which helps in forging action at the trailing edge of the shoulder. The penetration depth of the tool into material was approximately 1.9 mm from the top of the pin. For a metallurgical analysis, the specimens were grounded, polished, and etched according to ASTM E3-01. Chemical etching was performed using Keller's reagent. The FSPed specimens thickness was reduced from 6 mm to 2 mm (the backside of the specimens were machined to extract just the FSPed part). Then, the tensile test specimens were cut in the direction perpendicular to the weld line according to ASTM E8 standard.

3. Simulation Details

In this work, Deform-3D^{TM} software was employed to simulate the FSW due to the capability of precise modeling of processes with severe plastic deformation and point tracking. Additionally, it was assumed that:

(1) The workpiece is modeled as a rigid visco-plastic material;
(2) The welding tool is rigid;
(3) A constant friction factor is used for tool-sheet interface;
(4) The thermal characteristics of the workpiece and tool are constant.

For the material model of AA5083, a rigid-viscoplastic temperature and strain-rate dependent model was utilized. The Arrhenius equation was used to describe the relationship between the strain rate, flow stress

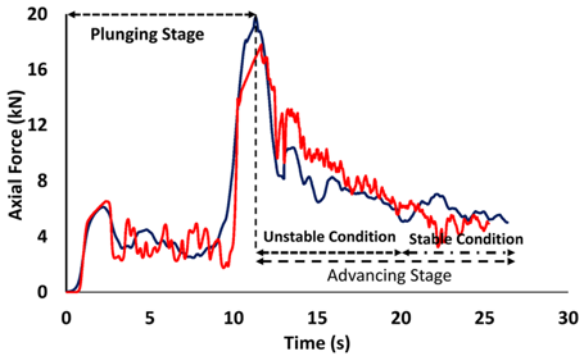

Fig. 1 Comparison of axial forces derived from the simulation and experimental results

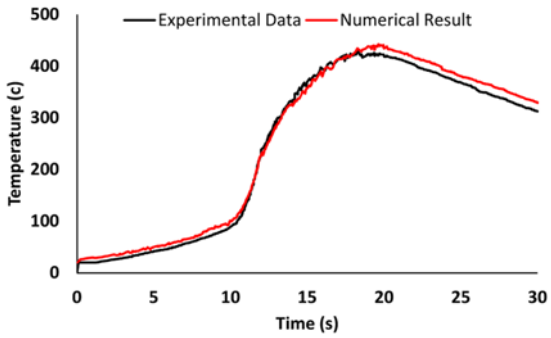

Fig. 2 Temperature histories derived from simulation and experiment

and temperature.[11] The constant shear friction model was used to model contact between tool and workpiece.[8,11] A comparison between the numerical and experimental results for welding forces is shown in Fig. 1; showing a good agreement between the predicted force and experimental data.

The simulation was performed at tool rotational speeds of 500, 700, 900, 1120, 1400 and 1600 rpm and traverse speeds of 18, 30, 42 and 60 mm/min in order to investigate the effects of tool traverse and rotational speeds.

4. Results and Discussion

In order to validate the accuracy of the simulation results, the temperature distribution found via simulation were compared with the experimental results, as shown in Fig. 2. The comparison shows the simulation results are in good agreement with the experimental data.

4.1 Effect of rotational speed on temperature

Fig. 3 shows temperature profile along transverse section of the weld zone for different rotational speed. It is observed from this figure that temperature distribution about the weld line is nearly symmetric for all rotational speeds. This is in line with the results reported by Buffa et al..[7] They stated that temperature profile along a transverse section is symmetric because the heat generation during FSW is dominated by tool rotating speed which is much higher than the traverse speed.

As shown from this figure with increasing tool rotational speed,

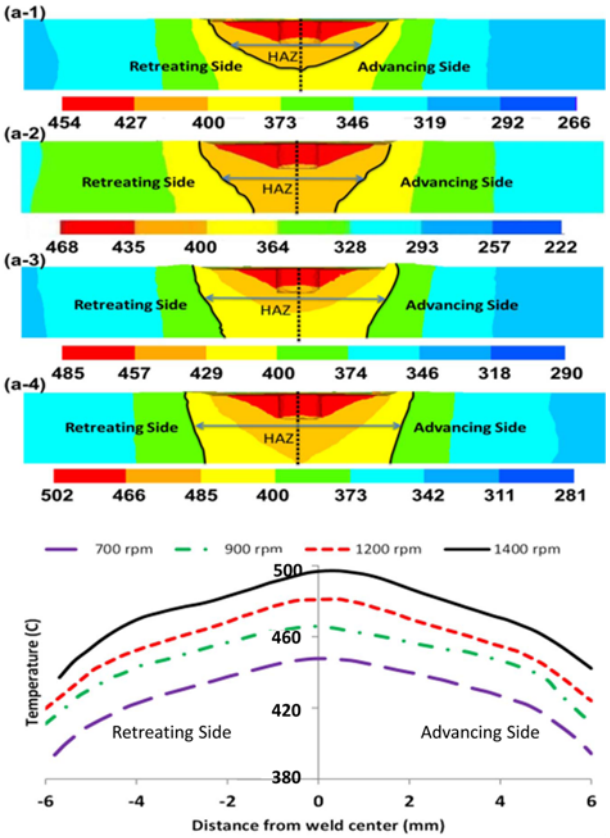

Fig. 3 Temperature profiles in the weld zone for the constant traverse speed of 30 mm/min and different rotational speeds of (a-1) 700 rpm, (a-2) 900 rpm, (a-3) 1200 rpm, and (a-4) 1400 rpm

both an expansion of the heat affected zone (HAZ) and a higher value of peak temperature can be seen. Higher value of maximum temperature in the FSW joint is favorable for the solid diffusion and plasticized mixing, and hence, is helpful for weld quality in terms of material ow. On the other hand, expansion of the HAZ, the most capable zone for fracture, decreases weld quality. Therefore, an optimum rotational speed is existed that provide high peak temperature in the weld zone and doesn't expand HAZ extensively. It must be noted that in this investigation, HAZ is considered as a zone experiencing a temperature rise above 400 C according to Buffa et al. work.[12]

4.2 Effect of traverse speed on temperature distribution

Fig. 4 shows temperature profile along transverse section of the weld zone for different traverse speed. As shown from this figure with decreasing tool traverse speed, both an expansion of the heat affected zone (HAZ) and a higher peak temperature value can be seen. The increase of temperature can be mainly ascribed to the increased time to heat up and weld the same length.

4.3 Welding force (transverse force)

In FSW, the tool experiences welding forces due to viscous and inertial effects. The welding forces are important for several reasons. First, tool wear are increased with increasing welding force leading to greater processing cost due to more frequent tool replacement. Second, tool wear may lead to weld contamination and worsen of the weld

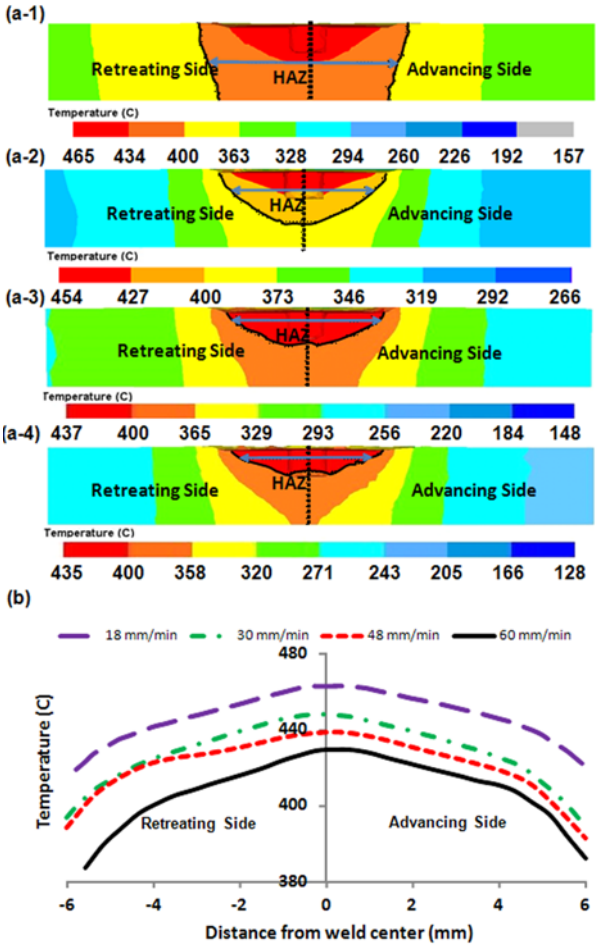

Fig. 4 The temperature profile in the weld zone at constant rotational speed of 700 rpm for different traverse speeds of (a-1) 18 mm/min, (a-2) 30 mm/min, (a-3) 42 mm/min, and (a-4) 60 mm/min

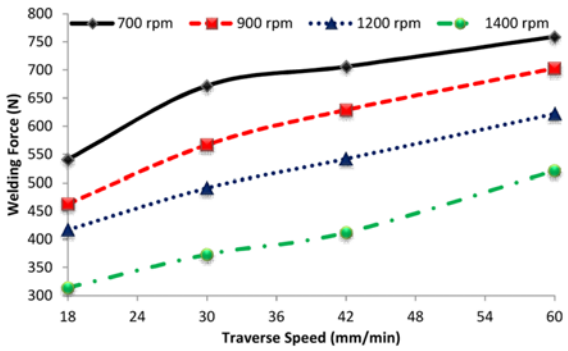

Fig. 5 The numerical welding forces for different traverse and rotational speeds

properties. Fig. 5 shows the numerical welding forces for different rotational and traverse speeds. As shown in the figure, welding forces decrease signicantly with increasing rotational speed or decreasing traverse speed, and this may lead to an increase in the tool lifetime. This is attributed to providing sufficient heat in order to material softening of the workpiece which decreases the resistant force against the tool as traverses along the weld line.

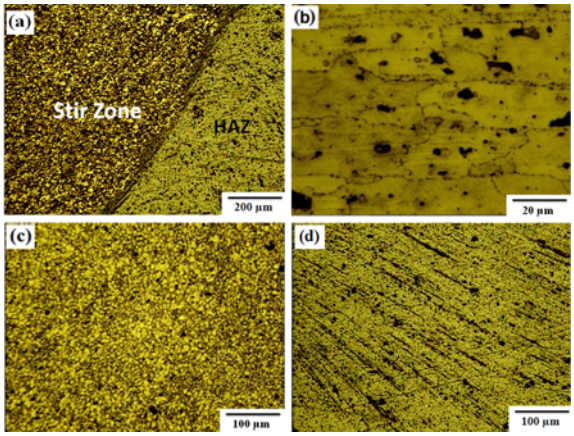

Fig. 6 Optical micrographs of transverse section of (a) transition zone, (b) HAZ, (c) nugget zone, and (d) TMAZ

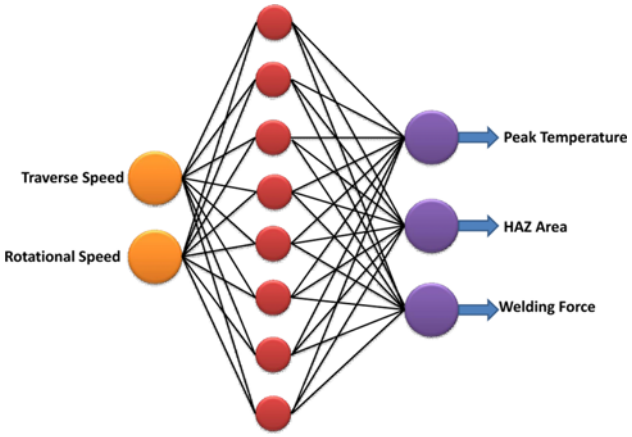

Fig. 7 Three layer neural network

4.4 Microstructural result

According to the optical microscopic investigations and based on the microstructural characterization of grains and precipitates, three distinct zones namely, (1) stirred zone (SZ), nugget zone (NZ) or dynamically recrystallized zone (DXZ); (2) thermo-mechanically affected zone (TMAZ), and (3) heat-affected zone (HAZ) were identied.[5]

Within stirred zone, intense plastic deformation and frictional heating during FSW/FSP result in generation of a recrystallized, ne-grained microstructure (Fig. 6a & 6c). It is well accepted that the dynamic recrystallization during FSP/FSW results in the generation of ne and equiaxed grains in the nugget zone. FSP/FSW parameters, initial temperature of the plates, and tool geometry are various parameters aecting the recrystallization in the SZ. The recrystallization could be reduced by decreasing the tool rotation rate at a constant welding speed or decreasing the ratio of the tool rotation/welding speed.[2,4,5] The TMAZ experiences both temperature and deformation during FSW/FSP (Fig. 6d). The TMAZ is characterized by a highly deformed structure. This zone on each side of the nugget, comprises of interfaces with the grains obtained from dynamic recrystallization process in the nugget zone and the base material.[13] Far from the weld is the HAZ, beyond which the base metal remains unaected. This zone experienced a thermal cycle but did not undergo any plastic deformation (Fig. 6b).[14] The HAZ has the lowest strength due to significantly coarsened precipitates. Thus, during tension, strain occurs mainly in the HAZ. Therefore, fracture always occurs in the HAZ, resulting in a low strength and ductility in transverse orientation of the weld.[5,15]

5. Modeling using Neural Networks

In this research, totally 24 different welding condition have been investigated in Deform-3DTM software which about 450 h was totally spent for computation. As result, friction stir welding simulation with different welding condition is very time consuming. Therefore, ANN was employed to model FSW with the aim of achieving the required results without consuming much time. In this work, feed forward neural network with back-propagation algorithm has been used to model the relationship between welding parameters (traverse and rotational speeds) and HAZ width, peak temperature and welding force values.

To get the best neural network architecture, several architectures were evaluated. Based on this analysis, a 2-8-2 NN was selected as the optimal architecture and both activation functions in hidden layer and output layer were ‘logsig’. Schematic of this three layer neural network is shown in Fig. 7.

In this model, 80% of the total data randomly was employed for training stage, while the 20% was reserved for testing stage. The correlation coefficients (R^2) for peak temperature, force and HAZ width at the training and testing stages were 0.99, 0.999 and 0.9989 and 0.9721, 0.985 and 0.9645, respectively. It is clear that the neural network prediction is in very good agreement with the simulation results and the developed ANN can accurately predict peak temperature, force and HAZ.

6. Multi-Objective Optimization

In order to find optimum values of traverse and rotational speeds a hybrid multi-objective evolutionary algorithm is employed.[5] This proposed method consists of two stages: generation of a Pareto front by NSGA-II, and then using TOPSIS to obtain the best compromise solution from the Pareto set.

In many multi-objective optimization problems, the objectives are usually in conict with each other. Therefore, it is not possible to obtain a solution that minimizes (maximize) each objective concurrently. One answer for these problems consists of a set of solutions, called Pareto optimal. Pareto optimal is a solution which is not dominated by any other solution in the solution space. Pareto optimal solution cannot be improved with respect to an objective unless at least another objective is deteriorated.

In order to deal with this multi-objective optimization problem, a multi-objective evolutionary algorithm is used. To generate a Pareto-optimal solution, Non-dominated Sorting Genetic Algorithm (NSGA-II), was employed. The NSGA-II makes use of a fast non-dominated sorting approach, elitist strategy, and a crowded comparison operator to create Pareto-optimal solutions. First a random parent population is created. Binary tournament selection, recombination, and mutation

operators are employed to produce a child population. Then, a combined parent and child population is formed. This allows parent population to be compared with the child solution, thereby ensuring elitism. The population is sorted according to non-domination. The new same size parent population is formed according to non-domination ranks and crowded comparison operator. This population is now employed for selection, crossover and mutation to produce a new population. The detailed algorithm is reported in Ref. 16.

TOPSIS was employed to rank the given alternatives of the Pareto optimal solutions obtained by NSGA-II introduced by Hwang and Yoon.[17] The basic concept of TOPSIS finds the positive ideal solution (S^+) as well as the negative ideal solution (S.), and then determines the best compromise solution, which is the closest to S^+ and the farthest from S., from the Pareto optimal solution according to the decision maker's objective weights. The detailed algorithm is presented in our pervious works.[5,17]

6.1 Multi-objective optimization of friction stir parameter

In order to determine optimal traverse and rotational speeds the feed forward neural network model obtained in the previous section are now deployed in these three-objective optimization problems using NSGA-II algorithm.[5,18] A population size of 100 and a generation number of 500 were used in different runs where crossover probability P_c and mutation probability P_m were 0.7 and 0.07, respectively. The three conicting objectives in this study were peak temperature, HAZ width and welding force to be simultaneously optimized with respect to the design variables, namely rotational speed (R) and traverse speed (T). The optimization problem can be formulated as follow:

$$\begin{cases} \text{Maximize} & \textit{Peak Temperature} = f_1(R,T) \\ \text{Minimize} & \textit{HAZ Area} = f_2(R,T) \\ \text{Minimize} & \textit{Welding Force} = f_3(R,T) \\ \text{Subject to} & 500 \le \text{Rotational Speed} \le 1400 \\ & 18 \le \text{Traverse Speed} \le 60 \end{cases} \quad (1)$$

The non-dominated individuals of the three-objective optimization in different planes were shown in Fig. 8. It should be noted that there is a single set of individuals as a result of the three-objective optimization that are shown in different planes of objective function. Thus, there are some points in each plane that may dominate others in the same plane. However, these individuals are all non-dominated when considering all three objectives simultaneously. If the design variables (rotational and traverse speed) are chosen, based on the Pareto front, it leads to the best possible combination of those three objectives. It is now desired to obtain a trade-off optimum points out of non-dominated three-objective optimization process compromising all objective functions. This can be done by TOPSIS method described in Ref. 5. TOPSIS method is applied on the individuals obtained in three-objective optimization process. In this way, equal weights are employed to consider non-preference for all functions.[5,17] Table 2 depicts four optimum design points achieved by applying TOPSIS.

Consequently, there are some important optimal design facts among the objective functions which discovered by the multi-objective optimization of the ANN meta-models obtained using the numerical analysis of the FSW.

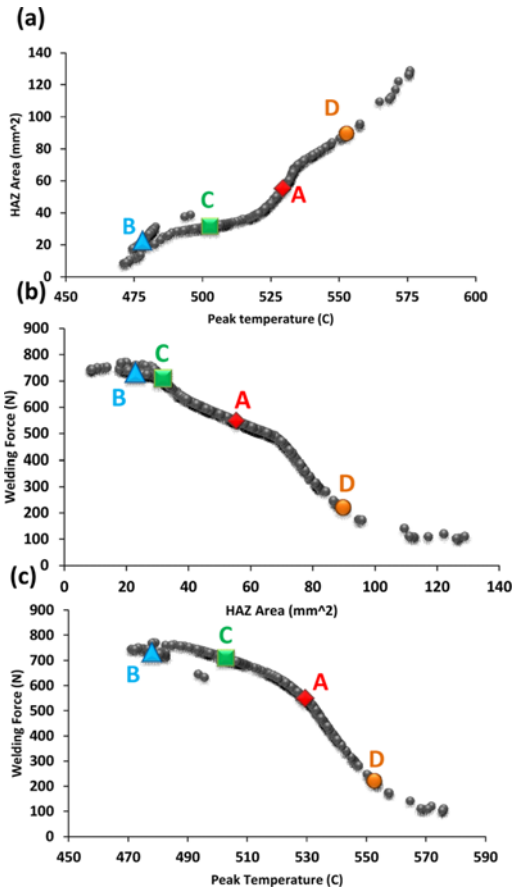

Fig. 8 Non-dominated individuals of the three-objective optimization in different planes (a) HAZ vs. peak temperature (b) welding force vs. HAZ (c) welding force vs. peak temperature

Table 2 The best compromise solutions determined by TOPSIS

Point	Rotational Speed (rpm)	Traverse Speed (mm/min)	Peak Temperature (°C)	HAZ width (mm)	Welding Force (N)
A	1344.599	59.753	529.3366	55.29098	548.8909
B	553.621	42.901	477.9437	22.77745	732.75
C	882.719	57.773	502.7696	31.68555	709.8935
D	1393.059	32.137	552.6367	89.62572	220.7031

Table 3 Weld efficiency in the FSWed samples produced by different process parameters

Sample No.	Rotational speed (rpm)	Traverse speed (mm/min)	Weld efficiency (%)
1	1345	60	91
2	550	45	89.5
3	600	40	85.6
4	1500	40	79

Two batches of optimum parameters, listed in Table 2, along with two batches of non-optimum parameters were employed to produce FSPed samples. Then the fabricated samples were conducted to tensile test. The tensile test efficiency of the welds is listed in Table 3, where the samples number 1 and 2 were produced according to the optimum parameters (points A and B in Table 2) and samples 3 and 4 according to non-optimum parameters. As can be concluded from Table 3, the

optimum process parameters based on three factors of peak temperature, HAZ width and welding force, results in higher weld efficiency.

7. Conclusions

In this investigation a thermo-mechanically coupled, 3D FEM analysis was used to investigate the effect of rotational and traverse speeds on welding force, peak temperature and HAZ width. Then an ANN model was employed to model the correlation between the welding parameters (rotational and traverse speeds) and welding force, peak temperature and HAZ width. Furthermore, the hybrid multi-objective optimization was used to determine the optimum values of rotational and traverse speeds. This method consists of two stages: generation of a Pareto front by NSGA-II, and using TOPSIS to obtain the best compromise solution from the Pareto front. Finally, by the obtained optimum process parameters, FSP samples were produced and conducted to tensile test which showed higher weld efficiency in compare with the samples produced by non-optimum parameters.

The result of present research can be summarized as follows:

1 - Expansion of the HAZ width along with the higher peak temperature will be revealed as the results of increasing rotational speed or decreasing traverse speed.

2 - Welding force decreases signicantly with increasing the rotational speed or decreasing the traverse speed and this may lead to an increase in tool lifetime.

3 - The training algorithm of back-propagation is sufficient for predicting peak temperature, HAZ width and welding force for different rotational and traverse speeds, and consequently reduces the computing time.

REFERENCES

1. Behnagh, R. A., Besharati Givi, M., and Akbari, M., "Mechanical Properties, Corrosion Resistance, and Microstructural Changes during Friction Stir Processing of 5083 Aluminum Rolled Plates," Materials and Manufacturing Processes, Vol. 27, No. 6, pp. 636-640, 2012.
2. Akbari, M. and Behnagh, R. A., "Dissimilar Friction-Stir Lap Joining of 5083 Aluminum Alloy to CuZn34 Brass," Metallurgical and Materials Transactions B, Vol. 43, No. 5, pp. 1177-1186, 2012.
3. Asadi, P., Givi, M. B., Rastgoo, A., Akbari, M., Zakeri, V., and Rasouli, S., "Predicting the Grain Size and Hardness of AZ91/SiC Nanocomposite by Artificial Neural Networks," The International Journal of Advanced Manufacturing Technology, Vol. 63, No. 9-12, pp. 1095-1107, 2012.
4. Akbari, M., Abdi Behnagh, R., and Dadvand, A., "Effect of Materials Position on Friction Stir Lap Welding of Al to Cu," Science and Technology of Welding and Joining, Vol. 17, No. 7, pp. 581-588, 2012.
5. Shojaeefard, M. H., Behnagh, R. A., Akbari, M., Givi, M. K. B., and Farhani, F., "Modelling and Pareto Optimization of Mechanical Properties of Friction Stir Welded AA7075/AA5083 Butt Joints using Neural Network and Particle Swarm Algorithm," Materials & Design, Vol. 44, pp. 190-198, 2013.
6. Shojaeefard, M. H., Akbari, M., Tahani, M., and Farhani, F., "Sensitivity Analysis of the Artificial Neural Network Outputs in Friction Stir Lap Joining of Aluminum to Brass," Advances in Materials Science and Engineering, Vol. 2013, Document ID: 574914, 2013.
7. Buffa, G., Hua, J., Shivpuri, R., and Fratini, L., "A Continuum based FEM Model for Friction Stir Welding-Model Development," Materials Science and Engineering: A, Vol. 419, No. 1, pp. 389-396, 2006.
8. Shojaeefard, M. H., Khalkhali, A., Akbari, M., and Asadi, P., "Investigation of Friction Stir Welding Tool Parameters using FEM and Neural Network," Proceedings of the Institution of Mechanical Engineers, Part L: Journal of Materials Design and Applications, DOI: 10.1177/1464420713509075, 2013.
9. Kim, D., Badarinarayan, H., Kim, J. H., Kim, C., Okamoto, K., et al., "Numerical Simulation of Friction Stir Butt Welding Process for AA5083-H18 Sheets," European Journal of Mechanics-A/Solids, Vol. 29, No. 2, pp. 204-215, 2010.
10. Buffa, G., Fratini, L., and Micari, F., "Mechanical and Microstructural Properties Prediction by Artificial Neural Networks in FSW Processes of Dual Phase Titanium Alloys," Journal of Manufacturing Processes, Vol. 14, No. 3, pp. 289-296, 2012.
11. Asadi, P., Mahdavinejad, R. A., and Tutunchilar, S., "Simulation and Experimental Investigation of FSP of AZ91 Magnesium Alloy," Materials Science and Engineering: A, Vol. 528, No. 21, pp. 6469-6477, 2011.
12. Buffa, G., Hua, J., Shivpuri, R., and Fratini, L., "Design of the Friction Stir Welding Tool using the Continuum based FEM Model," Materials Science and Engineering: A, Vol. 419, No. 1, pp. 381-388, 2006.
13. Mishra, R. S, and Ma, Z., "Friction Stir Welding and Processing," Materials Science and Engineering: R: Reports, Vol. 50, No. 1, pp. 1-78, 2005.
14. Shojaeefard, M. H., Khalkhali, A., Akbari, M., and Tahani, M., "Application of Taguchi Optimization Technique in Determining Aluminum to Brass Friction Stir Welding Parameters," Materials & Design, Vol. 52, No. pp. 587-592, 2013.
15. Mahoney, M. W., Rhodes, C. G., Flintoff, J. G., Bingel, W. H., and Spurling, R. A., "Properties of Friction-Stir-Welded 7075 T651 Aluminum," Metallurgical And Materials Transactions A, Vol. 29, No. 7, pp. 1955-1964, 1998.
16. Coello, C. A. C., "A Comprehensive Survey of Evolutionary-based Multiobjective Optimization Techniques," Knowledge and Information systems, Vol. 1, No. 3, pp. 269-308, 1999.
17. Etghani, M. M., Shojaeefard, M. H., Khalkhali, A., and Akbari, M., "A Hybrid Method of Modified NSGA-II and Topsis to Optimize Performance and Emissions of a Diesel Engine using Biodiesel," Applied Thermal Engineering, Vol. 59, No. 1, pp. 309-315, 2013.